FRP adhesive lap-joints: a micro-scale mechanical approach.

Francesco Ascione[1], Geminiano Mancusi[2]

[1]*Department of Civil Engineering, University of Rome "Tor Vergata", Italy*
E-mail: *ascione@ing.uniroma2.it*

[2]*Department of Civil Engineering, University of Salerno, Italy*
E-mail: *g.mancusi@unisa.it*

Keywords: Adhesive lap-joints, FRP, Couple stress theory.

SUMMARY. A micro-scale mechanical model for predicting the response of adhesive lap-joints between FRP adherents has been developed. Numerical results obtained via FEM method show the main features of such a behaviour. Comparisons with other results available in literature are also presented.

1 INTRODUCTION

As it is well-known, when dealing with thin films the size effect (i.e. the thinner, the stiffer) is often observed [1-2]. Such an effect also occurs in the case of adhesive interfaces between FRP profiles, where the glue layer can be few μm thick. Due to the lack of internal material length scale parameters, classical models are unable to capture the microstructure dependent size effect and, therefore, need to be extended by using high order non-local continuum theories.

Both the classical couple stress elasticity theory elaborated by Koiter [3] as well as several other higher-order elasticity theories available in literature [4-8] include four material constants: two classical and two additional. In particular, the two additional parameters, related to the symmetric and antisymmetric part of the curvature tensor, cannot be determined from single experiments as the twisting of a thin cylinder or the pure bending test of a thin film. Combinations of both types of tests are required.

In order to overcome the difficulties related to the evaluation of two microstructure length scale parameters [9-10], a modified couple stress theory has been recently developed by means of restricting the couple stress tensor to be symmetric [11]. As a consequence, the strain energy does not depend on the antisymmetric part of the curvature tensor and, therefore, only one additional material length scale parameter is required.

Based on this modified couple stress theory, several one-dimensional models have been recently proposed for studying both the Bernoulli-Euler [12] and Timoshenko [13] beam problems.

In this paper the modified couple stress theory [11] has been applied to study the behaviour of FRP adhesive lap-joints under axial loads. In particular, two-dimensional elastic fields have been introduced in order to simulate the response of both the adherents (plane stress) and the adhesive films (plane strain). In the latter, the mechanical model takes into consideration the internal material length scale parameter too.

The study proposed by the authors also accounts for the most common interfacial cohesive laws available in literature [14-17] as well as the simplified cohesive law proposed in [18]. In general, elastic moduli of the thin adhesive layers, in fact, are updated step-by-step in such a way that the current value of the elastic strain energy density is related to the corresponding value of the interface energy density, which depends on the cohesive mixed-mode fracture law considered.

The goal is to investigate the ultimate behaviour of FRP adhesive lap-joints by extending the numerical investigation previously developed by the authors in [19-20], where the micro scale effect has been neglected.

2 THE MODIFIED COUPLE STRESS THEORY: A BRIEF REVIEW

High order theories establish that the material particle is able not only to translate, as in classical continuum mechanics, but also to rotate and deform. As a consequence, the usual conception of a material particle as a geometric mass point is inadequate. The main feature is that the kinetic energy of a material particle depends on its tangential and rotational velocities. In particular, when dealing with static equilibrium, in addition to the classical equation involving applied forces, a new equation needs to be introduced between couples acting on a generic material particle.

When examining a system of material particles, unlike classical mechanics, a couple no longer behaves as a free vector, but as a driving force that rotates the material particle. As a result, not only are conventional force equilibrium and moment equilibrium equations (eqs.1.a-b) required, but also a moment of couples equilibrium equation (eqn. 1.c) is necessary [11].

$$\sum_{i=1}^{N}\mathbf{F_i}=\mathbf{0},\quad \sum_{i=1}^{N}\left[\left(\mathbf{x_i}-\mathbf{x_o}\right)\wedge\mathbf{F_i}+\mathbf{L_i}\right]=\mathbf{0},\quad \sum_{i=1}^{N}\left[\left(\mathbf{x_i}-\mathbf{x_o}\right)\wedge\mathbf{L_i}\right]=\mathbf{0}. \tag{1.a-c}$$

In the previous eqs.1.a-c, the symbol N indicates the number of material particles, $\mathbf{F_i}$ denotes the force vector applied to the generic *i-th* particle, $\mathbf{L_i}$ represents the couple vector, $\mathbf{x_i}-\mathbf{x_o}$ indicates the distance vector to the generic *i-th* particle from an arbitrary pole, O.

With respect to a continuum, the first two equilibrium equations (1.a-b) can be replaced as follows:

$$\int_V \rho\mathbf{b}\,\mathrm{dv}+\int_{\partial V}\mathbf{t_n}\,\mathrm{ds}=\mathbf{0}, \tag{2.a}$$

$$\int_V\left[(\mathbf{x}-\mathbf{x_o})\wedge\rho\mathbf{b}+\rho\mathbf{m}\right]\mathrm{dv}+\int_{\partial V}\left[(\mathbf{x}-\mathbf{x_o})\wedge\mathbf{t_n}+\boldsymbol{\mu}_\mathbf{n}\right]\mathrm{ds}=\mathbf{0}, \tag{2.b}$$

where V indicates an arbitrary volume of a deformable body bounded by piecewise smooth surfaces denoted by ∂V, the symbol $\mathbf{n}$ denotes the outer normal to the boundary surface ∂V, $\mathbf{b}$ and $\mathbf{m}$ denote, respectively, the body force and the body couple (per unit mass), ρ is the mass density, $\mathbf{x}-\mathbf{x_o}$ denotes the distance vector of a generic particle from an arbitrary pole O. Finally, $\mathbf{t_n}$ and $\boldsymbol{\mu}_\mathbf{n}$ denote, respectively, the traction and couple (per unit surface) acting on the boundary of the deformable body. According to Koiter [3], it is possible to refer to:

$$\mathbf{t}=\mathbf{T}\mathbf{n},\quad \boldsymbol{\mu}=\mathbf{M}\mathbf{n}, \tag{3.a-b}$$

where $\mathbf{T}$ is the stress tensor and $\mathbf{M}$ is the couple stress tensor. Using the divergence theorem to transform the surface integrals in eqs. 2.a-b, we obtain:

$$\int_V(\rho\mathbf{b}+\mathrm{Div}\,\mathbf{T})\,\mathrm{dv}=\mathbf{0}, \tag{4.a}$$

$$\int_V\left[\mathrm{Div}\,\mathbf{M}+\rho\mathbf{m}+2\mathbf{w}_\mathrm{T}\right]\mathrm{dv}=\mathbf{0}. \tag{4.b}$$

In eqn. 4.a-b the symbol $\mathbf{w}_T$ represents the following vector:

$$\mathbf{w}_T = -\frac{1}{2} e_{ijk} \mathbf{T}_{jk} \hat{\mathbf{e}}_i, \tag{5}$$

where $\hat{\mathbf{e}}_i$ denotes the generic unit vector (i=1, 2, 3).

Since the volume V is arbitrary, the volume dependence can be eliminated which then leads to:

$$\text{Div } \mathbf{T} + \rho \mathbf{b} = \mathbf{0} \qquad \text{in V,} \tag{6.a}$$

$$\text{Div } \mathbf{M} + \rho \mathbf{m} + 2\mathbf{w}_T = \mathbf{0} \qquad \text{in V.} \tag{6.b}$$

Finally, by manipulating the following additional equilibrium equation for moment of couples:

$$\int_V \left[(\mathbf{x} - \mathbf{x}_o) \wedge \left(\rho \mathbf{m} + 2\mathbf{w}_T \right) \right] \mathrm{dv} + \int_{\partial V} \left[(\mathbf{x} - \mathbf{x}_o) \wedge \boldsymbol{\mu}_n \right] \mathrm{ds} = \mathbf{0}, \tag{7}$$

it is possible to obtain the following expression:

$$\int_V \left[\mathbf{A} \left(\text{Div } \mathbf{M} + \rho \mathbf{m} + 2\mathbf{w}_T \right) + 2\mathbf{w}_M \right] \mathrm{dv} = \mathbf{0}. \tag{8}$$

In eqn. 8, $\mathbf{A}$ indicates the skew tensor related to the vector $(\mathbf{x} - \mathbf{x}_o)$ and $\mathbf{w}_M$ denotes the following vector:

$$\mathbf{w}_M = -\frac{1}{2} e_{ijk} \mathbf{M}_{jk} \hat{\mathbf{e}}_i. \tag{9}$$

By substituting eqn. 6.b into eqn. 8, it descends that the couple stress tensor **M** is symmetric.

3 PRINCIPLE OF VIRTUAL DISPLACEMENTS

In this section the deformation measures of the mechanical model are derived via the application of the principle of virtual displacements by assuming the strain energy, w, as a function of the gradients of translation, $\nabla \mathbf{u}$, and rotation, $\nabla \boldsymbol{\theta}$:

$$\int_V \delta w \left(\nabla \mathbf{u}, \nabla \boldsymbol{\theta} \right) \mathrm{dv} = \int_V \left(\rho \mathbf{b} \cdot \delta \mathbf{u} + \rho \mathbf{m} \cdot \delta \boldsymbol{\theta} \right) \mathrm{dv} + \int_{\partial V} \left(\mathbf{t}_n \cdot \delta \mathbf{u} + \boldsymbol{\mu}_n \cdot \delta \boldsymbol{\theta} \right) \mathrm{ds}. \tag{10}$$

Considering eqs. 3.a-b and applying the divergence theorem, by some algebra we can rewrite eqn. 10 as follows:

$$\int_V \delta w \left(\nabla \mathbf{u}, \nabla \boldsymbol{\theta} \right) \mathrm{dv} = \int_V \left[\left(\rho \mathbf{b} + \text{Div } \mathbf{T} \right) \cdot \delta \mathbf{u} + \left(\rho \mathbf{m} + \text{Div } \mathbf{M} \right) \cdot \delta \boldsymbol{\theta} + \right. \\ \left. + \mathbf{T} \cdot \nabla \delta \mathbf{u} + \mathbf{M} \cdot \nabla \delta \boldsymbol{\theta} \right] \mathrm{dv} \tag{11}$$

By substituting 6.a-b in eqn.11, we can obtain:

$$\int_V \delta \mathrm{w}\left(\nabla \mathbf{u}, \nabla \boldsymbol{\theta}\right) \mathrm{dv} = \int_V \left[\boldsymbol{\sigma} \cdot \delta \boldsymbol{\varepsilon} + \bar{\mathbf{m}} \cdot \delta \boldsymbol{\chi}\right] \mathrm{dv}, \tag{12}$$

where the following relationships have been used:

$$\boldsymbol{\varepsilon} = \frac{1}{2}\left[\nabla \mathbf{u} + \left(\nabla \mathbf{u}\right)^{\mathrm{T}}\right], \quad \boldsymbol{\omega} = \frac{1}{2}\left[\nabla \mathbf{u} - \left(\nabla \mathbf{u}\right)^{\mathrm{T}}\right], \quad \boldsymbol{\theta} = -\frac{1}{2}\, \mathrm{e}_{\mathrm{ijk}} \boldsymbol{\omega}_{\mathrm{jk}} \hat{\mathbf{e}}_{\mathrm{i}} \tag{13.a-c}$$

$$\boldsymbol{\chi} = \frac{1}{2}\left[\nabla \boldsymbol{\theta} + \left(\nabla \boldsymbol{\theta}\right)^{\mathrm{T}}\right], \quad \boldsymbol{\gamma} = \frac{1}{2}\left[\nabla \boldsymbol{\theta} - \left(\nabla \boldsymbol{\theta}\right)^{\mathrm{T}}\right], \tag{13.d-e}$$

$$\boldsymbol{\sigma} = \frac{1}{2}\left(\mathbf{T} + \mathbf{T}^{\mathrm{T}}\right), \quad \boldsymbol{\tau} = \frac{1}{2}\left(\mathbf{T} - \mathbf{T}^{\mathrm{T}}\right), \tag{13.f-g}$$

$$\mathbf{M} = \mathrm{a}\,\mathbf{I} + \bar{\mathbf{m}}, \qquad \mathrm{a} = \frac{1}{3} tr(\mathbf{M}), \qquad \bar{\mathbf{m}} = \mathbf{M} - \mathrm{a}\,\mathbf{I}, \quad tr\left(\bar{\mathbf{m}}\right) = 0. \tag{13.h-k}$$

In deriving eqn.12 from eqn.11, the following further relationships have been invoked:

$$\boldsymbol{\tau} \cdot \delta \boldsymbol{\omega} - 2\mathbf{w}_{\mathrm{M}} \cdot \delta \boldsymbol{\theta} = 0, \quad \mathrm{a}\,\mathbf{I} \cdot \delta \boldsymbol{\chi} = 0. \tag{14.a-b}$$

4 PROBLEM FORMULATION

In order to study the behaviour of adhesive lap-joints, a specific model has been developed by assuming only two non-trivial displacement field components are present: *u* and *v*, along x and y axes, respectively. Adherents and adhesive layers are assumed to behave according to plane stress and plane strain hypotheses, respectively.

$$\boldsymbol{\sigma} = \begin{bmatrix} \sigma_{\mathrm{xx}} & \sigma_{\mathrm{xy}} & 0 \\ \sigma_{\mathrm{xy}} & \sigma_{\mathrm{yy}} & 0 \\ 0 & 0 & 0 \end{bmatrix}, \qquad \bar{\mathbf{m}} = \begin{bmatrix} 0 & 0 & \mathrm{m}_{\mathrm{xz}} \\ 0 & 0 & \mathrm{m}_{\mathrm{yz}} \\ \mathrm{m}_{\mathrm{xz}} & \mathrm{m}_{\mathrm{yz}} & 0 \end{bmatrix}. \tag{15.a-b}$$

$$\boldsymbol{\varepsilon} = \begin{bmatrix} \dfrac{\partial u}{\partial x} & \dfrac{1}{2}\left(\dfrac{\partial u}{\partial y} + \dfrac{\partial v}{\partial x}\right) & 0 \\ \dfrac{1}{2}\left(\dfrac{\partial u}{\partial y} + \dfrac{\partial v}{\partial x}\right) & \dfrac{\partial v}{\partial y} & 0 \\ 0 & 0 & 0 \end{bmatrix}, \qquad \boldsymbol{\chi} = \begin{bmatrix} 0 & 0 & -\dfrac{1}{4}\left(\dfrac{\partial^2 u}{\partial x \partial y} - \dfrac{\partial^2 v}{\partial x^2}\right) \\ 0 & 0 & -\dfrac{1}{4}\left(\dfrac{\partial^2 u}{\partial y^2} - \dfrac{\partial^2 v}{\partial x \partial y}\right) \\ -\dfrac{1}{4}\left(\dfrac{\partial^2 u}{\partial x \partial y} - \dfrac{\partial^2 v}{\partial x^2}\right) & -\dfrac{1}{4}\left(\dfrac{\partial^2 u}{\partial y^2} - \dfrac{\partial^2 v}{\partial x \partial y}\right) & 0 \end{bmatrix} \tag{15.c-d}$$

Orthotropic constitutive relationships are utilized. In particular, in the case of the adhesive layers, the microstructure length scale parameter, *l*, has been considered too. The following relationships exist:

$$\varepsilon_{\mathrm{xx}} = \frac{1}{\mathrm{E}_{\mathrm{xx}}}\sigma_{\mathrm{xx}} - \frac{\nu_{\mathrm{xy}}}{\mathrm{E}_{\mathrm{xx}}}\sigma_{\mathrm{yy}} \qquad \varepsilon_{\mathrm{yy}} = -\frac{\nu_{\mathrm{xy}}}{\mathrm{E}_{\mathrm{xx}}}\sigma_{\mathrm{xx}} + \frac{1}{\mathrm{E}_{\mathrm{yy}}}\sigma_{\mathrm{yy}} \qquad \varepsilon_{\mathrm{xy}} = \frac{1}{2\mathrm{G}_{\mathrm{xy}}}\sigma_{\mathrm{xy}} \tag{16.a-c}$$

$$m_{xz} = 2l^2 G_{xy} \chi_{xz} \qquad m_{yz} = 2l^2 G_{xy} \chi_{yz} \qquad (16.d\text{-}e)$$

Some geometrical details are presented in the following Figure 1. It is important to highlight the condition $h_a << b_a$ which allows the adhesive layer to be studied under the well-known plane strain hypotheses.

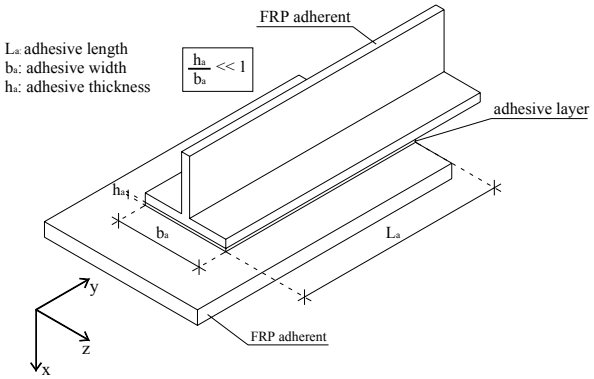

Figure 1: Generic scheme of an adhesive joint.

The most common cohesive interface models available in literature [14-17] are simulated by updating elastic moduli of adhesive. In particular, the strain components ε_{xx} and ε_{xy} can be related to mode I and mode II interface displacements, respectively:

$$\varepsilon_{xx} = \frac{\delta_n}{h_a} \qquad \varepsilon_{xy} = \frac{1}{2}\frac{\delta_s}{h_a} \qquad (17.a\text{-}b)$$

where h_a (Fig. 1) indicates the thickness of the adhesive layer, while δ_n and δ_s the normal and tangential interfacial displacements, respectively. Furthermore, the stress component σ_{yy} is assumed to be equal to zero:

$$\sigma_{yy} = 0. \qquad (18)$$

As a consequence the normal, t_n , and tangential, t_s, interface interactions can be easily related to the strain components ε_{xx} and ε_{xy}. It results:

$$t_n = \sigma_{xx} = E_{xx}\varepsilon_{xx} = \left(\frac{E_{xx}}{h_a}\right)\delta_n \qquad t_s = \sigma_{xy} = 2G_{xy}\varepsilon_{xy} = \left(\frac{G_{xy}}{h_a}\right)\delta_s \qquad (19.a\text{-}b)$$

It is worth noting the terms within brackets on the right hand side of eqs. 19 represent the current secant slopes for Mode I and Mode II cohesive law, respectively (Figs. 2.a-b).

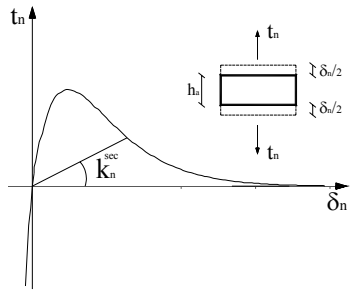

Figure 2.a: Mode I cohesive law.

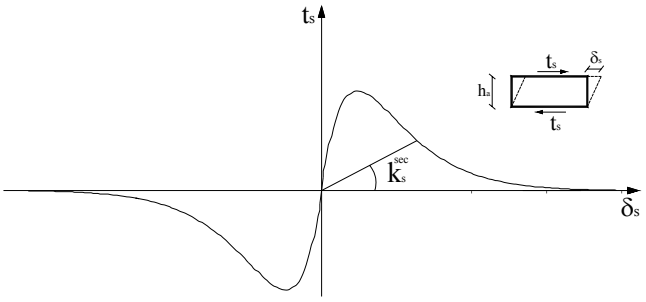

Figure 2.b: Mode II cohesive law.

Despite E_{xx} and G_{xy}, which are step-by step updated in order to account for the non-linearity of the cohesive laws, the quantity $l^2 G_{xy}$ can be assumed not dependent on the current values of inter-facial interactions.

5 FEM MODEL

In this section a finite element approximation of the proposed mechanical problem is developed. A 8-nodes finite element mesh has been introduced over both the adherents and the adhesive layers. Cubic interpolant shape functions [21] are utilized to approximate the displacement field components u_i and v_i (i=1, 2, ..., 8) over each finite element:

$$N_1(\xi,\eta)=\frac{1}{4}(1-\xi)(1-\eta)(-1-\xi-\eta) \qquad N_2(\xi,\eta)=\frac{1}{2}(1-\xi^2)(1-\eta) \qquad (20.a\text{-}b)$$

$$N_3(\xi,\eta)=\frac{1}{4}(1+\xi)(1-\eta)(-1+\xi-\eta) \qquad N_4(\xi,\eta)=\frac{1}{2}(1-\xi)(1-\eta^2) \qquad (20.c\text{-}d)$$

$$N_5(\xi,\eta)=\frac{1}{2}(1+\xi)(1-\eta^2) \qquad N_6(\xi,\eta)=\frac{1}{4}(1-\xi)(1+\eta)(-1-\xi+\eta) \qquad (20.e\text{-}f)$$

$$N_7(\xi,\eta)=\frac{1}{2}(1-\xi^2)(1+\eta) \qquad N_8(\xi,\eta)=\frac{1}{4}(1+\xi)(1+\eta)(-1+\xi+\eta). \qquad (20.g\text{-}h)$$

In the previous equations, ξ and η denote the local co-ordinates relative to the master finite element shown in Figure 3; they are related to the absolute co-ordinates by the following relationships:

$$x=x_o+\frac{L_x}{2}\xi \qquad (-1\le\xi\le 1) \qquad\qquad y=y_o+\frac{L_y}{2}\eta \qquad (-1\le\eta\le 1) \qquad (21.a\text{-}b)$$

where L_x and L_y are the actual lengths of the finite element along the x and y axes, respectively, and pedix "O" refers to the centroid of the finite element.

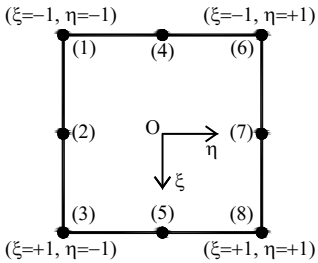

Figure 3: Master finite element.

The equilibrium of each finite element can be formulated by using the virtual displacements principle. With reference to the generic *e-th* finite element, it results:

$$\delta \mathrm{L}_{\mathrm{int}}^{(e)} = \mathbf{v}^{(e)\,T}\ \mathbf{K}^{(e)}\ \delta\mathbf{v}^{(e)} \qquad\qquad \delta L_{\mathrm{ext}}^{(e)} = \mathbf{f}^{(e)}\ \delta\mathbf{v}^{(e)} \qquad\qquad (22.\text{a-b})$$

where:

$$\mathbf{K}^{(e)} = \frac{L_x\, L_y}{4}\int_{-1}^{+1} d\xi \int_{-1}^{+1} d\eta \left[\mathbf{B}^{(e)T}\mathbf{C}^{(e)}\ \mathbf{B}^{(e)}\right] \qquad \mathbf{f}^{(e)} = \left[\mathrm{f}_{\mathrm{x},1},\, \mathrm{f}_{\mathrm{y},1},\, ...,\, \mathrm{f}_{\mathrm{x},8},\, \mathrm{f}_{\mathrm{y},8}\right]^{\mathrm{T}} \qquad \mathbf{v}^{(e)} = \left[u_1,\, v_1,\, ...,\, u_8,\, v_8\right]^{\mathrm{T}} \qquad (23.\text{a-c})$$

In particular, the numeric quantities $\mathrm{f}_{\mathrm{x,i}}$ and $\mathrm{f}_{\mathrm{y,i}}$ denote the components of the external force applied at the generic *i-th* node, along x and y axes, respectively; $\mathbf{B}^{(e)}$ is a 5x16 numeric matrix relating the five strain components ε_{xx}, ε_{yy}, ε_{xy}, χ_{xz}, χ_{yz} to the nodal displacements vector $\mathbf{v}^{(e)}$; $\mathbf{C}^{(e)}$ is a 5x5 numeric matrix relating the five stress components σ_{xx}, σ_{yy}, σ_{xy}, $\bar{\mathrm{m}}_{xz}$, $\bar{\mathrm{m}}_{yz}$ to the above listed strain components.

Finally, from the expressions of the matrices $\mathbf{K}^{(e)}$ and the vector $\mathbf{f}^{(e)}$, by a standard procedure, it is easy to obtain the global system of equations governing the equilibrium of the FEM model. Due to the mathematical expression of the cohesive laws considered [14-17], this system can be solved by means of an iterative algorithm which updates, at every step, the global secant stiffness matrix of the FEM model.

6 NUMERICAL RESULTS AND DISCUSSION

In this section some numerical results, obtained by using the finite element procedure above described, are presented and discussed. The numerical experiments developed not only allow to make comparisons with other results currently available in literature in order to assess the accuracy of the numerical procedure, but also highlight the influence of the micro-scale parameter on the behaviour of a balanced double-lap joint.

6.1 Comparisons with one-dimensional beam models

The two-dimensional FEM model here proposed, which accounts for the microstructure length scale parameter *l*, has been validated by means of some comparisons with numerical solutions currently available in literature, dealing with static beam problems: the Bernoulli-Euler beam problem

studied by Park and Gao [12] and the Timoshenko beam problem analyzed by Ma et al. [13] have been considered (Figs. 4). Geometric and mechanical properties are summarized in Table 1.

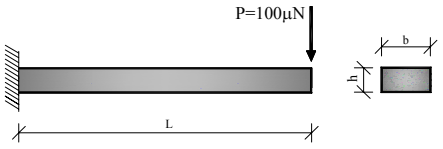

Figure 4.a: Cantilever beam.

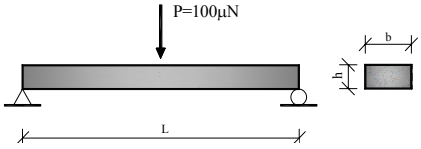

Figure 4.b: Simply supported beam.

Table 1: Geometric and mechanical properties assumed in [12-13].

	Case	**E**	ν	l	**h**	**b=2h**	**L=20h**
		[GPa]		[μm]	[mm]	[mm]	[mm]
Cantilever beam	I	1.44	0.38	0.0	0.0200	0.0400	0.4000
	II				0.0380	0.0760	0.7600
	III				0.0750	0.1500	1.5000
	IV				0.1150	0.2300	2.3000
	V			17.6	0.0200	0.0400	0.4000
	VI				0.0380	0.0760	0.7600
	VII				0.0750	0.1500	1.5000
	VIII				0.1150	0.2300	2.3000
Simply supported beam	IX	1.44	0.38	0.0	0.0176	0.0352	0.3520
	X				0.0352	0.0704	0.7040
	XI				0.0704	0.1408	1.4080
	XII			17.6	0.0176	0.0352	0.3520
	XIII				0.0352	0.0704	0.7040
	XIV				0.0704	0.1408	1.4080

The mesh adopted by the authors is as follows: two divisions along the vertical axis (x); forty divisions along the longitudinal axis (y). A specific test has been developed in order to assess the convergence of the solution obtained by the authors (a). The following Table 2 presents the results of a comparative analysis in terms of maximum deflection, f.

Table 2: Comparisons in terms of beam deflection f.

		Cantilever beam (mm $\cdot 10^2$)								**Simply supported beam** (mm $\cdot 10^3$)					
l **[μm]**	Case	I	II	III	IV	V	VI	VII	VIII	IX	X	XI	XII	XIII	XIV
0.0	$f^{(a)}$	5.55^1 5.56^2 5.55^3	2.92^1 2.93^2 2.92^3	1.48^1 1.48^2 1.48^3	0.96^1 0.97^2 0.97^3	-	-	-	-	3.97^1 3.97^2	1.98^1 1.98^2	0.99^1 0.99^2	-	-	-
	$f^{(b)}$	5.56	2.92	1.48	0.97	-	-	-	-	-	-	-	-	-	-
	$f^{(c)}$	-	-	-	-	-	-	-	-	2.14^4 3.97^5	1.07^4 1.98^5	0.53^4 0.99^5	-	-	-
17.6	$f^{(a)}$	-	-	-	-	4.17^1 3.88^2 1.27^3	2.32^1 2.21^2 1.51^3	1.29^1 1.28^2 1.20^3	0.89^1 0.89^2 0.88^3	-	-	-	2.98^1 2.71^2	1.56^1 1.45^2	0.86^1 0.82^2
	$f^{(b)}$	-	-	-	-	1.27	1.51	1.20	0.88	-	-	-	-	-	-
	$f^{(c)}$	-	-	-	-	-	-	-	-	-	-	-	0.65^4 0.57^5	0.68^4 0.79^5	0.47^4 0.72^5

(a): Ascione & Mancusi
1 --- ν = 0.38 G = E / 2 (1+ν)
2 --- ν = 0.00 G = E / 2
3 --- ν = 0.00 G = ∞

(b): Park & Gao

(c): Ma & al.
4 --- ν = 0.38 G = E / 2 (1+ν)
5 --- ν = 0.00 G = E / 2

It is important to remark that the additional modulus l^2G has been related to the actual value of the shear modulus (G=522 MPa) when considering cases V-IX (cantilever beam), without any dependency on the current choice assumed for G ($l^2G = 0.161614$ N). On the other hand, when considering cases XII-XIV (simply supported beam), it has been determined accounting for the current choice assumed for G: ($l^2G = 0.161614$ N or $l^2G = 0.223027$ N).

Results obtained by the authors (a) strictly agree with the solution (b) given in [12] if the Poisson modulus is assumed equal to zero and the shear modulus increases towards $+\infty$. On the contrary, they differ from the solution (c) given in [13]. Generally, the proposed two-dimensional model shows a lower size-effect than the Timoshenko beam model developed in [13].

6.2 *Influence of length micro-scale parameter on the behaviour of double lap-joints*

In this sub-section a numerical analysis of a balanced double-lap joint (Fig. 5) has been developed. Due to the low thickness of the adhesive interfaces between FRP adherents, very close to the value of the microstructure length scale parameter l, the authors propose to account for this parameter with respect to the adhesive layer in order to highlight its influence on the mechanical behaviour of the joint.

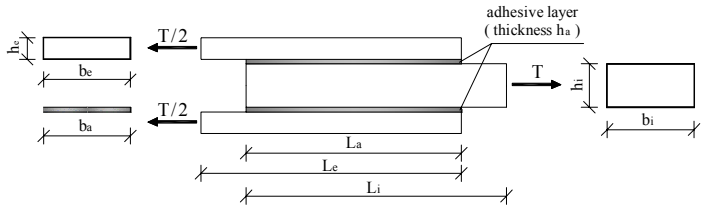

Figure 5: Balanced double lap-joint.

Although the mechanical model presented in section 4 allows to account for general cohesive interfacial laws, the example here discussed has been developed by adopting simplified laws characterized by a linear elastic branch up to failure (Fig. 6) subtending well-defined areas (fracture energy per unit surface), according to the procedure proposed in [18]. As a consequence, the non linear problem introduced in section 5 becomes a linear elastic one.

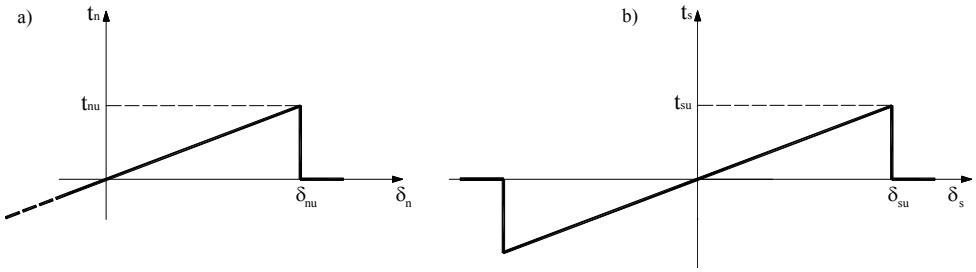

Figure 6: Simplified cohesive laws - a) Mode I; b) Mode II.

According to Hutchinson and Suo criterion [15], full separation between adherents is achieved when the following condition occurs:

$$\frac{G_I}{\Phi_I}+\frac{G_{II}}{\Phi_{II}}=1 \tag{24}$$

where:

$$G_I=\int_0^{\bar{\delta}_n} t_n d\delta_n \qquad \Phi_I=\int_0^{\delta_{nu}} t_n d\delta_n \qquad G_{II}=\int_0^{\bar{\delta}_s} t_s d\delta_s \qquad \Phi_{II}=\int_0^{\delta_{su}} t_s d\delta_s \tag{24.a-d}$$

It is worth noting that the symbols $\bar{\delta}_n$ and $\bar{\delta}_s$ indicate the current values of interfacial displacements δ_n and δ_s, respectively, while the symbols δ_{nu} and δ_{su} denote the ultimate values of such displacements. More details relating to the cohesive laws are summarized in Table 3.

Table 3: Mechanical parameters of cohesive laws.

δ_{nu}	$0.368 \cdot 10^{-1}$	mm		δ_{nu}	$0.343 \cdot 10^{-1}$	mm
t_{nu}	14.13	N/mm^2		t_{su}	28.28	N/mm^2

The geometric and mechanical properties of adherents and adhesive are summarized in Table 4, with reference to the symbols indicated in Figure 5. They are representative for common FRP profiles and epoxy resins currently available. Finally, the mesh details are presented in Table 5, where symbols n_x and n_y denote the number of divisions along the x and y axes, respectively, while L_x and L_y have the same meaning already introduced in section 5.

Table 4: Geometric and mechanical properties of adherents and adhesives.

	Geometric properties			**Elastic moduli**				
	Thickness	Width	Length	E_{xx}	E_{yy}	G_{xy}	ν_{xy}	l
	[mm]			[MPa]			[-]	[μm]
External adherents	$h_e=0.25$	$b_e=20.0$	$L_e=90.0$	7450	93700	3970	0.26	0
Internal adherent	$h_i=0.50$	$b_i=20.0$	$L_i=90.0$	7450	93700	3970	0.26	0
Adhesives	$h_a=0.02$	$b_a=20.0$	$L_a=80.0$	2500	2500	962	0.30	0-100

Table 5: Mesh details (measures in mm).

	un-bonded left region $0 \text{ mm} \le y \le 10 \text{ mm}$	**bonded region** $10 \text{ mm} < y \le 90 \text{ mm}$	**un-bonded right region** $90 \text{ mm} < y \le 100 \text{ mm}$
External adherents	$n_x=2\ (L_x=0.125)$ $n_y=100\ (L_y=0.10)$	$n_x=2\ (L_x=0.125)$ $n_y=800\ (L_y=0.10)$	-
Internal adherent	-	$n_x=4\ (L_x=0.125)$ $n_y=800\ (L_y=0.10)$	$n_x=4\ (L_x=0.125)$ $n_y=100\ (L_y=0.10)$
Adhesive Layers	-	$n_x=2\ (L_x=0.01)$ $n_y=800\ (L_y=0.10)$	-

The influence of the micro-scale length parameter l of the adhesive layer is shown in the last Table 6 where the ultimate axial load T_u has been related to the strength of the adhesive interface.

Table 6: Ultimate values of axial load T_u

	Case 1	Case 2	Case 3	Case 4
l [μm]	0.0	20.0	50.0	100.0
T_u [N]	5679	5937	6009	6055
Diff. [%]	-	+4.5	+5.8	+6.6

In particular, when the parameter l is supposed to be equal to the thickness of the adhesive layer (20 μm), as frequently occurs, the size effect provokes a significant increase in terms of the interface strength (+4.5%).

7 CONCLUSIONS

A two-dimensional micro-scale mechanical model for predicting the response of adhesive lap-joints between FRP adherents has been proposed. The model allows to simulate the interfacial interactions according to the most common cohesive laws available in literature. The influence on the joint mechanical behaviour of the microstructure length scale parameter of the adhesive layer has been investigated and the size-effect on the joint strength has been estimated. Results obtained by the authors show a significant increase in terms of joint strength when the influence of this parameter is accounted for.

References

[1] Lam, D.C.C., Yang, F., Chong, A.C.M., Wang, J. and Tong, P., "Experiments and theory in strain gradient elasticity" in *Int. J. Mech. Phys. Solids,* **51**, 1477-1508 (2003).

[2] McFarland, A.W. and Colton, J.S., "Role of material microstructures in plate stiffness with relevance to microcantilever sensors" in *Int. J. Micromech. Microeng.*, **15**, 1060-1067 (2005)

[3] Koiter, W.T., "Couple-stress in theory of elasticity: I and II" in *Proc. K. Ned. Akad. Wet*, **B67 (1)**, 17-44 (1964).

[4] Papargyri-Beskou, S., Tsepoura, K.G., Polyzos, D. and Beskos, D.E., "Bending and stability analysis of gradient elastic beams" in *Int. J. Solids Struct.* **40**, 385-400 (2003).

[5] Giannakopoulos, A.E. and Stamoulis, K., "Structural analysis of gradient elastic components" in *Int. J. Solids Struct.* **44**, 3440-3451 (2007).

[6] Peddieson, J., Buchanan, G.R. and McNitt, R.P., "Application of non local continuum models to nanotechnology" in *Int. J. Eng. Sci*. **41**, 305-312 (2003).

[7] Wang, Q., "Wave propagation in carbon nano tubes via non local continuum mechanics" in *J. Appl. Phys*. **98**, 124301, 1-6 (2005).

[8] Reddy, J.N., "Non local theories for bending, buckling and vibration of beams" in *Int. J. Eng. Sci*. **45**, 288-307 (2007).

[9] Lam, D.C.C., Yang, F., Chong, A.C.M., Wang, J. and Tong, P., "Experiments and theory in strain gradient elasticity" in *J. Mech. Phys. Solids* **51**, 1477-1508 (2003)

[10] Maranganti, R. and Sharma, P., "A novel atomistic approach to determine strain-gradient elasticity constants: tabulation and comparison for various metals, semiconductors, silica, polymers and the (ir) relevance for nanotechnologies" *J. Mech. Phys. Solids* **55**, 1823-1852 (2007)

[11] Yang, F., Chong, A.C.M., Lam, D.C.C. and Tong, P., "Couple stress based stain gradient theory of elasticity" in *Int. J. Solids Struct.*, **39**, 2731-2743 (2002).

[12] Park, S.K. and Gao, X.L., "Bernoulli-Euler beam model based on a modified couple stress theory" in *Int. J. Micromech. Microeng.*, **16**, 2355-2359 (2006).

[13] Ma, H.M., Gao, X.L. and Reddy J.N., "A microstructure-dependent Timoshenko beam model based on a modified couple stress theory" in *J. Mech. Phys. Solids*, **56**, 3379–3391 (2008).
[14] Suo, Z. and Hutchinson, J.W., "Interface crack between two elastic layers", *Int. J Fracture*, **43**, 1-18 (1990).
[15] Hutchinson, J.W. and Suo, Z., "Mixed-mode cracking in layered materials", *Adv Appl Mech*, **29**, 63-191 (1992).
[16] Xu, X.P. and Needleman A., "Void nucleation by inclusing debonding in a crystal matrix", *Modeling Simul. Mater. Sci. Eng.*, **1**, 111-132 (1993).
[17] Camacho, G. T. and Ortiz, M., "Computational modelling of impact damage in brittle materials", *Int. J Solids Struct*, **33**, 2899-2938 (1996).
[18] Ascione, F., "Mechanical behaviuor of adhesive lap joints", Proceedings of National congress AIMETA, Brescia (2007).
[19] Ascione, F. and Mancusi, G., "Axial/Bending coupled analysis for FRP adhesive lap-joints" in *Mech Adv Mater Struct* (in press).
[20] Ascione, F. and Mancusi, G., "Failure criteria for FRP adhesive lap-joints: a comparative analysis" in *Mech Adv Mater Struct* (in press).
[21] Reddy J. N., "An Introduction to Nonlinear Finite Element Analysis", New York, Oxford University Press, (2004).